Emission of Slow and Fast Electrons from Clean Metal Surfaces Under Impact of Slow Multicharged Ions

We discuss the interplay of various electron emission processes induced by impact of slow ($v_p \leq 10^5$ m/s) multicharged ions on an atomically clean metal surface, with prior emphasis on the resulting slow (≤ 50 eV) electron emission statistics (viz. the measured probability distributions for emission of given numbers of slow electrons). A recently developed classical overbarrier model satisfactorily describes the relevant electronic transitions between an incoming multicharged ion and the metal surface in the context of a four-stage scenario, i.e., (I) the projectile's approach toward the surface, (II) its close contact with the latter, (III) its subsequent penetration into the target bulk and finally, depending on impact energy and angle, (IV) its possible backscattering into vacuum. Slow electrons are mainly emitted during phases (I) and (II) and contribute dominantly to the observed total electron yields.

Key Words: *multicharged-ion surface interaction, hollow atoms, potential emission, multicharged ion neutralization, ion-induced electron emission*

1. INTRODUCTION

An ion which approaches a solid surface gives rise to a transient excited complex, because of the available ion recombination energy. Deexcitation of this short-lived complex can take place via various electronic transitions between states of the particle and the surface. Besides their fundamental interest, these processes are also of practical relevance for plasma–wall interaction in gas discharges including thermonuclear fusion experiments, ion beam-activated material modification and surface analytics involving elastic or inelastic ion beam scattering. For impact of neutral atoms

Comments At. Mol. Phys.
1994, Vol. 29, No. 5, pp. 275–303
Reprints available directly from the publisher
Photocopying permitted by license only

and/or singly charged ions, relevant electronic interactions have been studied during the last four decades in increasing detail.[1–6] For singly charged ions, the principal deexcitation mechanism usually involves Auger electron transitions between two electrons of the surface density-of-states (S-DOS, cf. list of abbreviations in the Appendix), by which means one of them may become ejected into vacuum, to give rise to "potential emission" (PE).[1] At sufficiently low ion impact energy the corresponding PE yield will dominate over also possible contributions from kinetic electron emission (KE). For impact of doubly charged ions, two electrons can be resonantly captured from the S-DOS, followed by autoionization of the such transiently formed neutral, doubly excited particles.[7] The latter processes have recently been studied in considerable detail[8–11] and are comparably well understood. However, for impact of multicharged ions A^{q+} (MCI, charge state $q > 2$), many different neutralization-deexcitation processes can become involved. Hagstrum[1,12] ($q \leq 5$) and Arifov *et al.*[13] ($q \leq 8$) first treated such cases both experimentally and theoretically. The latter authors assumed multiple-resonant transitions to take place between an incoming highly ionized particle and the metal surface, thus rapidly forming a multiply excited neutral particle, which then starts to decay via sequential autoionization processes, causing ejection of a corresponding number of slow electrons. In this way, the approaching particle becomes transiently converted into a "hollow atom" which carries a number of electrons in its outer shells, while its inner shells remain empty. With today's availability of powerful multicharged ion sources, production and decay of such "hollow atoms" near solid surfaces has become a subject of considerable interest.

Total yield and energy distributions of emitted electrons have been measured for impact of, e.g., Ar^{q+} ions up to $q = 12$.[14–16] It was found that for $q > 8$ the total slow electron yields no longer increased according to the MCI total recombination energy, as was the case for earlier results obtained with lower ion charge states.[13] Rather, in the course of the MCI's neutralization, some inner shell vacancies stay empty until close contact of the projectile with the target surface, and will even be carried into the target bulk where they finally decay under emission of fast Auger electrons, as first

demonstrated with H-like N^{6+} and O^{7+} projectiles.[17] Several groups[18–20] have studied the related Auger electron spectra in detail, and conversion of MCI into "hollow atoms" near a metal surface has also been demonstrated from the resulting soft X-ray emission.[21–24] In addition, fast Auger electrons can also originate from the target particles,[25] and the above described inner shell vacancies in recombining MCI influence the projectile-charge dependence of the charge states of both the scattered projectiles[26] and the sputtered target atoms.[27]

So far, reviews of this rapidly emerging field have mainly applied classical concepts,[13,28–30] and some of the involved electronic transitions have also been treated quantum mechanically, e.g., resonant neutralization (RN; Ref. 31) and autoionization (AI; Ref. 32).

Auger electron transitions within the transiently formed, multiply excited "hollow atoms" cause their autoionization ("AI") and are the more probable the smaller the change in principal quantum numbers for the respective "down-electrons".[13,29,30] Consequently, the bulk of the ejected "up-electrons" gain a kinetic energy of a few eV only, whereas the much faster "above-surface" (henceforth abbreviated as "a.s.") produced electrons due to Auger transitions into the projectile inner-shell vacancies remain comparably sparse. During further approach of the particle toward the surface, already emitted electrons can be replaced by the continuing RN which, however, will run into competition with other projectile ionization processes as, e.g., electron promotion into vacuum due to state shifting (which also produces a.s. slow electrons) and resonant ionization (RI) into empty surface states. A detailed discussion of these and other relevant transitions will be presented in Section 3.

However, as soon as the projectile has reached the surface, all of its electrons still bound in highly excited states will become stripped off[18,30] and in this way additional slow electrons will be produced.[33] When subsequently penetrating into the target bulk, the transiently reionized projectile will again become neutralized, but now only into more tightly bound shells which can still exist within the solid.[33] Because of this change in the projectile's population distribution, still present inner-shell vacancies can now be recombined with a much higher probability than above the surface,

which gives rise to the major share of observable fast Auger electrons, i.e., the so-called "below-surface" (henceforth abbreviated as "b.s.") fast Auger electron emission.[18,34] Secondary electrons produced inside the target bulk by the fast b.s. Auger electrons can also provide some slow electrons. Under favorable backscattering conditions some projectile inner-shell vacancies may even survive after the projectile has again left the target surface and become eventually filled above the latter, which produces additional a.s. fast Auger electrons.[20] In this Comment we would like to demonstrate that the number of ejected slow electrons greatly surpasses the number of fast Auger electrons, giving the former ones a dominant role for the observable total electron yields. In particular, we will regard data for total slow electron yields due to impact of very slow, highly charged ions (up to fully stripped Ar^{18+}, Li-like Xe^{51+} and Ne-like Th^{80+}, respectively) on a clean gold surface,[33,35] which have been determined by measuring the related electron emission statistics (ES), i.e., the probability distributions W_n for emission of $n = 0, 1, 2 \ldots$ electrons.[36]

2. PRACTICAL ASPECTS OF MEASURING SLOW MCI-INDUCED ELECTRON EMISSION FROM A CLEAN METAL SURFACE

In Figs. 1a and 1b we have sketched the presently most common experimental techniques for studying electron production due to impact of slow MCI on a solid surface via measuring, respectively, (a) the total electron yields, and (b) the kinetic energy spectra. Figures 1c–1e show further experimental approaches for studying such collisions via (c) the electron emission statistics, (d) projectile scattering and (e) the resulting soft X-ray emission. Reference 37 provides some guidance for the preparation of suitable slow MCI beams and of atomically clean metal target surfaces, for which we would like to emphasize some especially important points.

First of all, to obtain reliable experimental data in this field of research, preparation of well-defined target surfaces and conduction of the measurements under ultrahigh vacuum conditions are mandatory. This is of particular importance for all processes which

depend either directly or indirectly on electronic transitions in front of the surface, as the a.s. slow electron emission, the a.s. fast Auger electron emission and, most notably, the scattering of projectiles under grazing angles of incidence, for which almost perfectly flat target surfaces need to be prepared.[38] In a further context we will only regard such experimental results which have been obtained by meeting these stringent conditions. However, when studying fast b.s. Auger electrons or soft X-ray emission, the target surface cleanliness is less important, since both processes originate within the solid. Furthermore, one can apply either polycrystalline or single-crystalline target surfaces. In the latter case, additional information becomes available by aligning the MCI incidence with different low-index directions of the target crystal surface.[39] We emphasize the high desirability of comparing results obtained with different target species, since the influence of the latter properties (e.g., work function, electron density, conductivity) on MCI-induced electron emission phenomena has not been systematically investigated, so far.

In order to impose a low vertical impact velocity on the surface, in some studies relatively fast MCI are impacted under grazing incidence. We mention that such studies are subject to rather strong effects as Doppler shifting and modification of the S-DOS[3,5,6] and a strong KE background (see, e.g., Zeijlmans van Emmichoven *et al.*, *loc. cit.*, Ref. 18). Since KE produces low electron energy continua similar to the PE processes, such techniques are of limited use for detailed investigation of the PE contributions of our present interest.

A final remark is in order on the absolute measurement of slow electron energy distributions, which becomes rather difficult at an electron energy typically below 10 eV, since contact potential differences, spectrometer transmission characteristics, stray fields and incompletely defined collection geometries all pose considerable problems. Hemispherical retarding field analyzers as are common in low-energy electron-diffraction (LEED) surface studies instead of the electron spectrometers sketched in Fig. 1b provide the most reliable results, especially if the absolute yields of, respectively, slow and fast electrons need to be compared.[14,15,40]

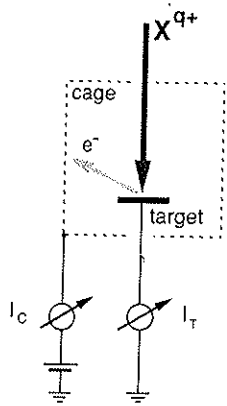
X^q+
cage
e⁻
target
I_C
I_T

(a)

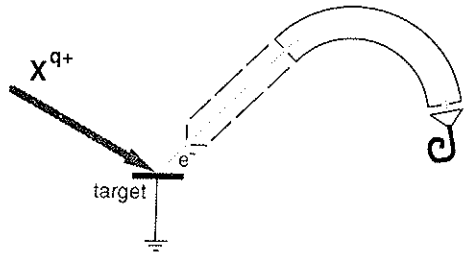
X^q+
e⁻
target

(b)

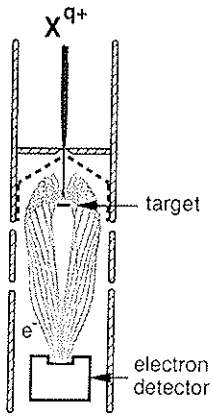
X^q+
target
e⁻
electron
detector

(c)

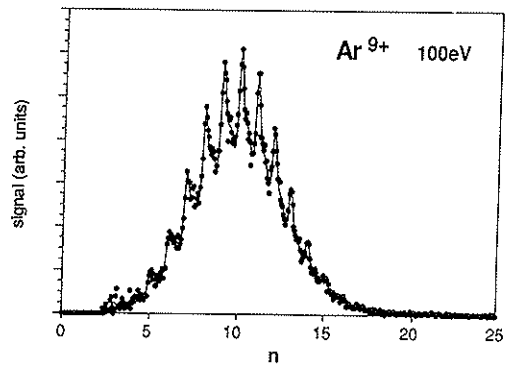
Ar 9+ 100eV
signal (arb. units)
0
5
10
15
20
25
n

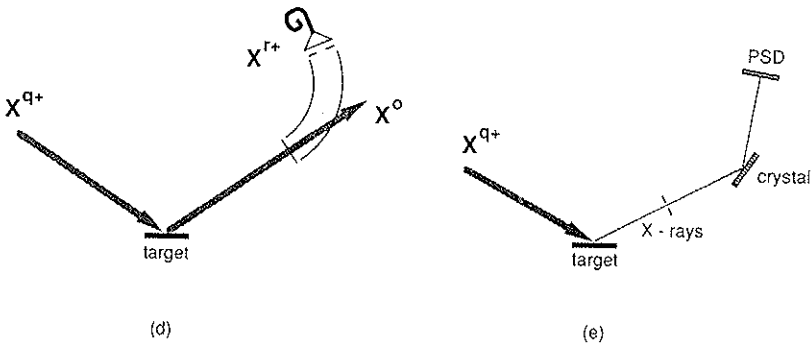

FIGURE 1 Standard experimental arrangements for the investigation of MCI–surface interaction. Abbreviations: X^{q+}: MCI-projectile of charge state q; e^{-}: emitted electrons; X^{r+}: scattered projectile of charge state r; X^{0}: scattered neutral particle; PSD: position sensitive detector; I_c: collector current; I_T: target current. (a) Measurement of total electron yields. (b) Spectroscopy of ejected electron energy distributions. (c) Measurement of electron emission statistics (ES) and typical example of measured ES (detector signal vs. electron multiplicity n) measured for 100 eV Ar^{9+} impact on clean Au (from Ref. 33). (d) Measurement of charge state and/or angular distributions of scattered projectiles. (e) Spectroscopy of emitted X-rays.

3. THE OVERALL SCENARIO OF SLOW MCI–METAL SURFACE INTERACTIONS AS BASED ON EXPERIMENTAL EVIDENCE

The until now developed scenario for the interaction of a MCI with a metal surface has evolved from numerous experimental investigations of total electron yields, electron emission statistics and fast Auger electron energy distributions, together with the analysis of scattered projectiles and soft X-ray emission. So far, it is best described in terms of the so-called "classical over-the-barrier model" (COB-model), which has recently been developed by J. Burgdörfer *et al.*[30] The approach of a slow MCI (charge state q; projectile velocity $v_p \ll v_F$, v_F being the Fermi velocity of electrons inside the metal target) toward a metal surface (usually characterized in the "jellium approximation" by a conduction band with the work function W_Φ and Fermi energy E_F, cf. Fig. 2) causes a collective response of the metal electrons, which under the above as-

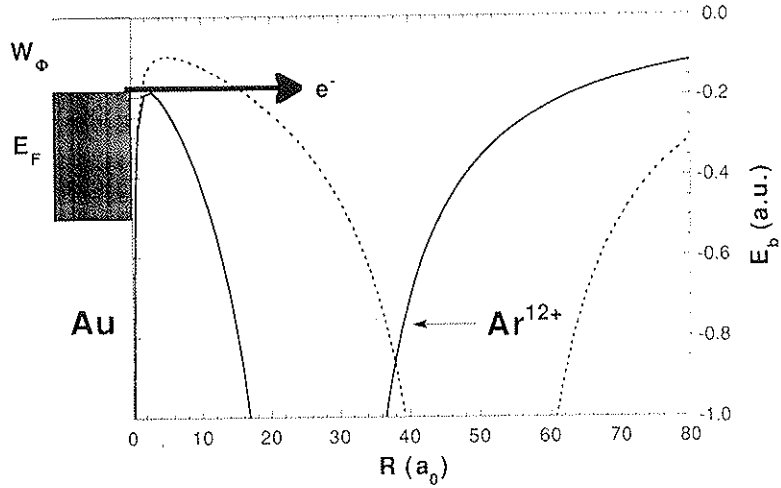

FIGURE 2 Electronic potential barrier between the MCI and the surface, exemplified for the cases of an Ar^{12+} projectile at about 50 a.u. (dotted curve) and 26 a.u. (full curve), respectively, above a Au surface. In the second case, the potential barrier has decreased below the Fermi level of Au, by which electron capture becomes classically permitted.

sumptions at large distance R can be described by the classical image potential (atomic units are used unless otherwise stated)

$$V_{\mathrm{im}}(R) = \frac{q^2}{4R}. \tag{1}$$

This image potential accelerates the MCI towards the metal surface and therefore imposes a lower limit to the projectile impact velocity, corresponding to an upper limit for the available MCI–surface interaction time. In addition, the image interaction causes a shift of the projectile electron states and decreases the height of the electronic potential barrier between the MCI and the surface (cf. Fig. 2 and Ref. 30), which is formed by the projectile's potential, its image potential and the image potential of the particular electron to be captured. At a critical distance $R_c(q)$,

$$R_c(q) = \frac{1}{2W_\Phi}\sqrt{8q + 2}, \tag{2}$$

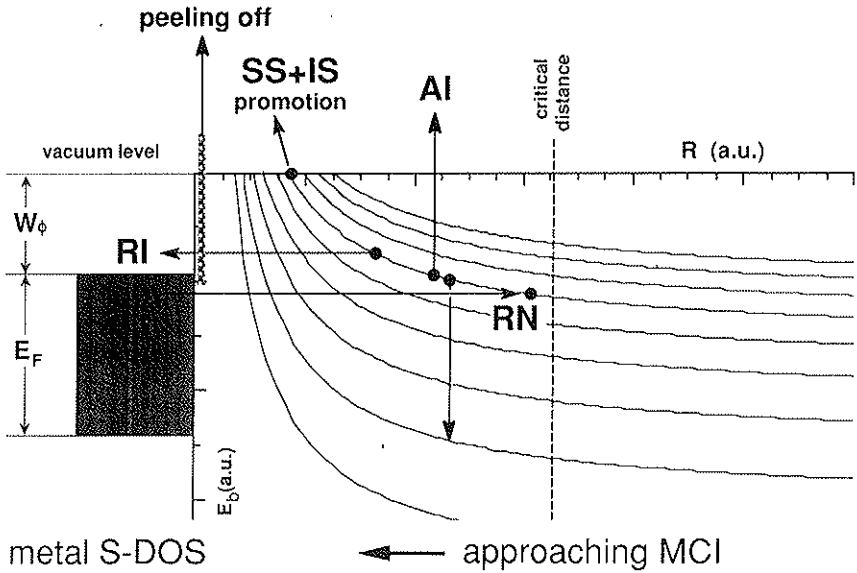

FIGURE 3 States of a neutralizing MCI approaching a metal surface. Electrons captured via RN can be emitted via AI, promotion into vacuum due to screening and image shift (SS/IS), and "peeling off" of all electrons which cannot stay bound to the projectile inside the solid. Furthermore, electrons can be recaptured into the solid via RI.

this potential barrier (cf. Fig. 2) will have decreased below the Fermi level of the metal, at which moment the MCI will start to capture electrons resonantly from near the Fermi edge of the conduction band (resonant neutralization, RN; cf. Fig. 3) into highly excited projectile states. Although electron capture is in principle already possible at larger distances via tunneling processes through the potential barrier, this has been found to be of minor importance.[30]

The COB model also predicts the principal quantum number of that highly excited projectile state in which this RN will take place:

$$n_c \leq \frac{q}{\sqrt{2W_\phi}}\left(1+\frac{q-0.5}{\sqrt{8q}}\right)^{-1/2}. \qquad (3)$$

The RN stops as soon as captured electrons have shielded the ion charge and, as a consequence, the potential barrier has moved up again above the Fermi level. With ongoing approach of the projectile, the over-the-barrier condition will be restored and RN can go on. However, the above mentioned image interaction and the screening of the projectile charge by already captured electrons will shift the energy levels of the projectile upwards ("image shift," IS and "screening shift," SS; see Fig. 3), because of which n_c in Eq. (3) designates the highest n-shell of the projectile which can be reached during the whole neutralization sequence.

The further evolution of the now multiply excited projectile depends on the competition between RN and other classes of electronic transitions. Intra-atomic Auger transitions involving two or more electrons already on the projectile lead to electron emission into vacuum (autoionization, AI) or into empty states above the Fermi level of the conduction band ("Auger-loss to the conduction band," AL), at the same time populating lower projectile n-shells (cf. Fig. 3). Electrons which have been shifted above the potential barrier and the Fermi level of the target surface can be lost into empty states of the conduction band (resonant ionization RI as the inverse process to RN), or become promoted above the vacuum level and thus emitted ("IS + SS promotion mechanism," cf. Fig. 3[30,33]). However, any electron lost from the projectile is rapidly replaced by RN, and eventually a fully neutralized "hollow atom" has been formed.

The complete deexcitation of this highly excited species to its neutral ground state, via the above described manifold of electronic interactions, would require a time not available because of the upper limit set by the image charge attraction (cf. above). At the end of phase I (approach toward the surface) the "hollow" projectile will thus touch the surface (phase II) still in a highly excited state, where now a third slow-electron emitting process (the so-called "peeling off mechanism," PO[30,33]) becomes operative, because screening of the projectile core by metal electrons within the first target layer causes the removal (i.e., "peeling off") of all the electrons with larger Rydberg radii $r_B = n^2/q$ than the screening length within the solid $\lambda_s = v_F/\omega_p$[41] of the metal (ω_p . . . surface plasmon frequency; $\lambda_s \approx 3$ a.u. for a gold target). However, the such

removed electrons will rapidly be replaced within the solid via electronic transitions like resonant capture of target core electrons and/or Auger neutralization (AN) by electrons from the conduction band into more tightly bound shells of the projectile, thus forming a much less excited "hollow" projectile. Very likely, these processes contribute to the slow electron yield as well, similar to the process of transfer ionization in MCI–atom collisions.

Further relaxation of the projectile within the solid (phase III) will finish with the filling of not yet recombined inner shell vacancies. As already outlined in Section 1, these transitions provide the majority of the observed fast (projectile) Auger electrons, in competition with also possible X-ray emission, according to the given fluorescence yield.

Alternatively, sufficiently close encounters of the projectile with target atoms can transfer some projectile vacancies to the target atom cores via quasi-RN or Fano–Lichten type promotion, resulting in the emission of characteristic target auger lines.[25] Fast Auger electrons emitted inside the solid either from the projectile or the target atoms may also produce slow secondary electrons. All the electrons (fast and slow) emitted during phase III are contributing to the b.s. PE. The projectiles will either remain inside the solid until their complete neutralization and stopping, or may be backscattered at any point on their trajectory within the target. In the case of grazing incidence, this backscattering corresponds to a "specular reflection" of the projectiles (cf. Ref. 6), in which case the projectile deexcitation will be completed on its outgoing trajectory.

A detailed modelling of the above sketched scenario has so far only been made for phase I. As an example, Fig. 4 illustrates a modelled evolution for Ar^{12+} ions impinging on clean gold ($W_\Phi = 5.1$ eV) with a nominal kinetic energy of 750 eV ($v \approx 6 \times 10^4$ m/s), exposing the following developments. At the critical distance $R_c \approx 26$ a.u. (cf. also Eqs. (2) and (3) and Figs. 2 and 3) electron capture into $n = 13$ starts, and soon thereafter AL will cause population into the $n = 12$ states (Fig. 4b). At $R \approx 21$ a.u., lowering of the potential barrier and IS of the $n = 12$ shell permit RN to proceed into it, because of which about six electrons will be quickly captured. The increased population of $n = 12$ screens the nuclear charge for the

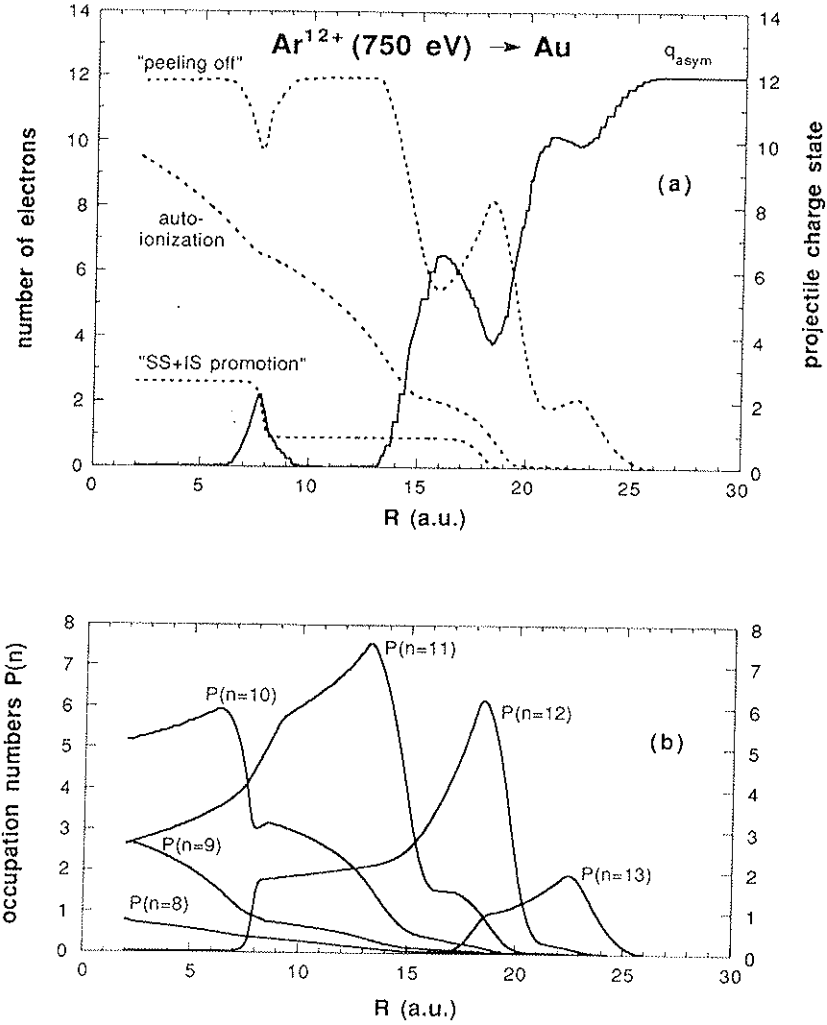

FIGURE 4 Modelled neutralization of a 750 eV Ar^{12+} ion ($v_p \approx 6 \times 10^4$ m/s) approaching a clean gold surface (from Ref. 33): (a) Evolution of asymptotic ion charge state q_{asym}, number of emitted electrons (autoionization and promotion) and number of electrons that will be emitted (peeled off) when the projectile hits the surface vs. projectile–surface distance. (b) Population of shells with principal quantum numbers $n = 8$–13.

electrons already occupying the $n = 13$ shell, and eventually—at $R \approx 18$ a.u.—causes promotion of these electrons into vacuum (cf. Fig. 4a). These concomittant processes continue for the $n = 12$, $n = 11$ and $n = 10$ shells. The simulation is stopped at a distance of $R = 2$ a.u. from the target, because neither the concept of image charge nor the assumption of hydrogenic energy levels remains appropriate in closer vicinity to a conducting surface. From $R \approx 13$ a.u. on, the initial Ar^{12+} projectile remains practically neutral (Fig. 4a) but carries all its captured electrons in highly excited states toward the surface, where 12 electrons will still be populating the $n = 8$ through $n = 11$ shells (cf. Fig. 4b). All these electrons are now peeled off, because the condition $r_B \leq \lambda_s$ permits only electrons with $n < 5$ to remain bound in projectile states inside the solid.

Only for an initial Ar^{12+} velocity $v_p < 10^4$ m/s (corresponding to 21 eV nominal impact energy, but 50 eV will be gained in addition due to the image charge attraction, see below) is there enough time for some electrons to reach the M- and N-shells. Of course, the projectile's evolution obtained from this modelling is more detailed than can (and probably ever will) be deduced from the possible experimental information, and it is thus of interest to which detail the above presented scenario is indeed unambiguously supported by available experimental evidence, as we will discuss in the following.

(i) Distance of First Neutralization

We start by examining the evidence for the distance of first electron capture as predicted by the COB model (Eq. (2)). This distance is closely related to the kinetic energy gain $\Delta E_{q,\mathrm{im}}$ of the projectile due to its image charge attraction, which accelerates the projectile until its complete neutralization. A simple staircase approximation within the COB model[30] predicts

$$\Delta E_{q,\mathrm{im}} \approx 0.236 \cdot W_\Phi \cdot q^{3/2} . \tag{4}$$

About 75% of this energy is already gained by the projectile on its way from infinity to the distance R_c of its first electron capture via RN (Eq. (2)). This image charge acceleration can be seen qualita-

tively from saturation effects with decreasing impact velocity, both for total electron yields[33] and a.s. K-shell Auger electron intensities.[18,34] Quantitative measurements of the corresponding energy gain are possible from the charge-state-dependent scattering angles of Ar^{q+} projectiles (q = 1–6) impinging under grazing angles on a clean, flat target surface.[38] Due to the image charge attraction, the ion velocity component perpendicular to the target surface will increase on the incoming path, resulting in a larger specular reflection angle for higher q than for initially neutral or less highly charged projectiles. Such measurements have recently been extended to Xe^{q+}-projectiles in charge states up to $q = 33$.[42] Good agreement was found with $q^{3/2}$ dependence as predicted by Eq. (4) about up to $q = 26$, beyond which the such determined image charge acceleration apparently became "saturated." It is important to note that this particular experimental technique depends on the assumption that the outgoing projectile trajectory itself is not subject to any image charge attraction, i.e., that reflected projectiles remain neutral from the outset. While this might be the case for moderately charged Ar^{q+} and Xe^{q+} ($q < 8$) projectiles, for much higher charged incident ions as, e.g., Xe^{30+}, some inner-shell vacancies might survive for a sufficiently long time after the surface scattering and thus decay only during phase IV, causing a recharging of the projectile and, at the same time, production of fast a.s. Auger electrons. Note, that such a recharging is probably responsible for the results of the scattering measurements by de Zwart *et al.*[26] (see Section (v) for a further explanation). Moreover, near the surface the PO mechanism transiently causes a charging up of the projectile, because of which the latter might appear as not fully neutralized on the very first part of its outgoing trajectory. "Saturation" of the measured $\Delta E_{q,\mathrm{im}}$ with increasing q as reported in Ref. 42 might be caused by this effect, since Xe^{q+} ions carry vacancies in their M-shells for $q > 26$.

Recently, Aumayr *et al.*[35] could extract $\Delta E_{q,\mathrm{im}}$ quantitatively from the leveling-off of measured total slow electron yields at low nominal projectile velocities ($< 3 \times 10^4$ m/s), for perpendicular impact of very highly charged ions (up to Th^{80+} and Xe^{51+}) onto a clean polycrystalline gold surface. As an example, for Th^{71+} projectiles they found a low impact energy limit of about 700 ± 160

eV (cf. Figs. 5a and 5b). The approximate validity of Eq. (4) could thus be confirmed up to the so far highest accessible MCI charge states. Consequently, the distance for the first electron capture seems to be quite well predicted by the COB model,[30] also in good agreement with classical dynamic calculations regarding the predominant neutralization processes.[43]

(ii) Auger Electron Emission Cascades

Direct experimental evidence for the development of such cascades is only available from their last few steps, i.e., the filling of K-shell or L-shell holes in the projectile, which can be unambiguously identified from the respective characteristic peaks in the fast electron energy spectra.[18–20,34] Doppler shift measurements of the relevant Auger lines were found consistent with an emission from projectiles still travelling along their original direction of incidence. In earlier work[16] all of these electrons were attributed to phase I, but more recent experiments showed that actually only a minor fraction of the inner-shell vacancies (typically less than 10%) are being filled above the surface,[18,34] whereas the majority of the fast Auger electrons is emitted from inside the metal, i.e., during phase III. The thus always minor a.s. contribution to the fast Auger electron peaks can only be absolutely determined in careful measurements at very low impact energy and/or with grazing-incident projectiles. As already mentioned, the fraction of these a.s. fast Auger electrons is limited by the image charge acceleration.[18,34]

The large majority of electrons emitted during phase I involves energies of a few eV only (cf. Ref. 33). From their broad, unstructured energy distribution it is not possible to assign the emission of slow electrons to specific AI transitions. However, a systematic comparison of measured total electron emission yields and statistics[33] with results of COB-modelling calculations can serve to separate the contribution of electrons generated by the AI-mechanism from other a.s. and b.s. slow electron emitting processes. Measured total yields for impact of slow (typical projectile velocities between 2×10^4 and 2×10^5 m/s) MCI as N^{q+} ($q = 5, 6$), Ne^{q+} ($q = 5–10$), Ar^{q+} ($q = 5–16$), Kr^{q+} ($q = 5–10$), Xe^{q+} ($q = 6, 8, 10$) and I^{q+}

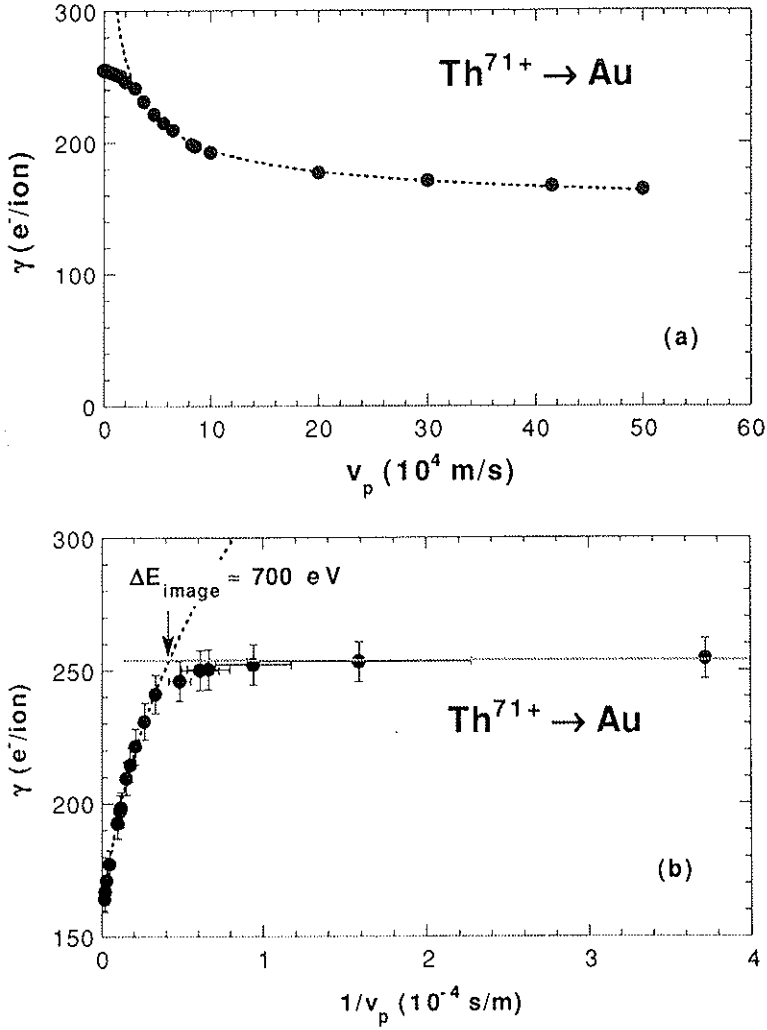

FIGURE 5 (a) Measured total electron yield λ vs. nominal (cf. text) projectile velocity v_p for impact of $^{232}Th^{71+}$ on clean polycrystalline gold (data from Ref. 35). (b) Same as (a) but plotted vs. the inverse nominal projectile velocity, in order to determine the image charge effect (cf. Ref. 35).

(q = 16, 20, 23, 25) on a clean polycrystalline gold surface were found first to gradually decrease with increasing impact velocity, but then to level off towards an apparent velocity-independent part of the total electron yield.[33]

Accompanying model calculations, as illustrated, e.g., in Fig. 6 for impact of Ar^{12+} on Au, indicated that the PO contribution to the total electron yield is nearly independent of the projectile's velocity (we remark that the IS/SS promotion mechanism was also found rather insensitive to v_p but, at least in this particular case, remained comparably unimportant), whereas the AI-related electron yield decreased with increasing projectile velocity, because of the decreasing time available for the AI cascades in front of the sur-

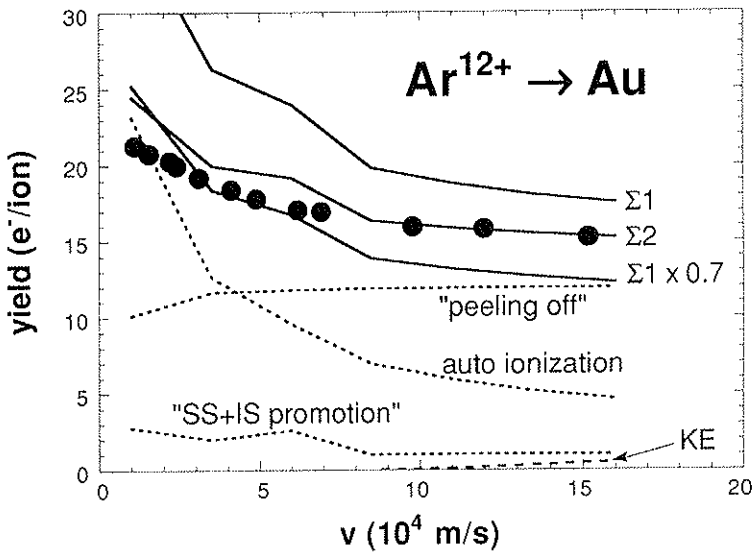

FIGURE 6 Total slow electron emission yields for impact of Ar^{12+} on gold vs. projectile velocity (from Ref. 33). Full symbols denote measured slow electron yields. Solid lines indicate the calculated total slow electron yields as derived under different assumptions for the fraction of electrons emitted from the projectile but absorbed by the Au surface (Σ1: no absorption, 0.7 × Σ1: 30% absorption of emitted electrons, Σ2: 50% of AI, but 0% of PO and IS/SS; for further details cf. Ref. 33.

face. Consequently, the velocity-dependent part of the total slow electron yield has to be attributed to AI (cf. Fig. 6). The measured functional dependencies of the total slow electron yields on the initial projectile charge state q could satisfactorily be reproduced by these modelling calculations. However, a quantitative comparison between the experimental yields and the corresponding simulated results is severely hampered not only due to an incomplete understanding of the b.s. slow electron contributions (they are estimated to be of minor importance in the case of slow Ar^{12+} on Au, however), but also from the unknown fraction of slow electrons which are emitted from the projectile toward the Au surface and there absorbed.

(iii) Evidence for the Peeling-Off Mechanism

The velocity-independence of the peeling-off contribution (cf. Fig. 6) results from the fact that the a.s. Auger transition cascade is much too slow for a significant population of such tightly bound levels which can stay filled when the projectile touches the surface. A "hollow" projectile which is neutral at the moment of surface impact should therefore lose practically all of its q electrons which still sit in outer shells. Experimentally, the velocity-independent slow-electron fraction of the total electron yield was found to increase more or less linearly with the initial projectile charge state q, but with a proportionality factor considerably larger than one.[33] The source of these extra electrons is still a matter of speculation, but since the related yields are proportional to q, it might result from AN-type processes which fill more tightly bound shells of the projectiles after the latter have just got peeled off their q outer electrons (cf. above). Comparison of measured slow-electron emission statistics (in particular their standard deviations[33]) with results of a Monte Carlo code version of the COB model gave further indications on the influence of a rather deterministic process like PO. These calculations showed that AI involves a relatively wide Gaussian-shaped probability distribution, while the PO mechanism in combination with IS/SS produces a rather narrow distribution, as was found appropriate to reproduce our recent experimental data[33] (cf. Fig. 7).

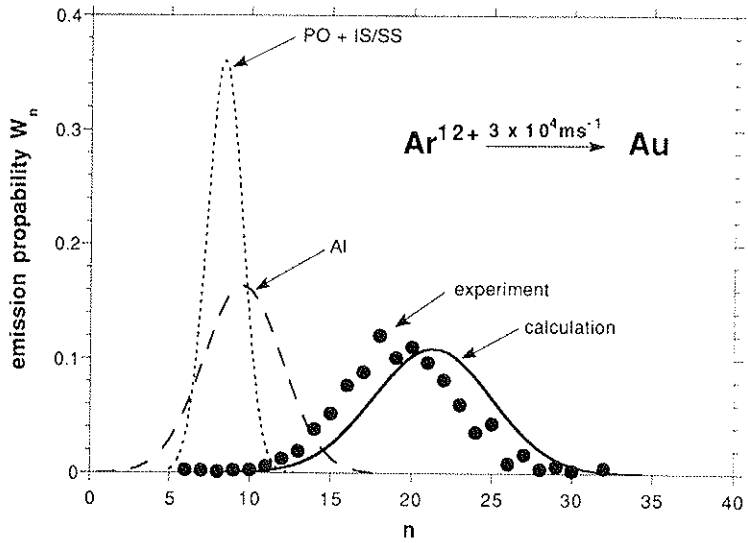

FIGURE 7 Modelled electron emission statistics (solid line) for impact of (nominally) 188 eV Ar^{12+} on clean gold, in comparison with the corresponding, experimentally obtained total statistics (full circles; data from Ref. 33). Individual contributions from Al and PO + IS/SS (dotted lines) are separately indicated.

(iv) Subsurface Deexcitation

Deexcitation of a projectile which is penetrating the solid involves a number of processes with different signatures. The appearance of characteristic target-Auger electron lines[25] proves that at least some projectile inner-shell vacancies survive sufficiently long to be transferred in close encounters to the target atoms. Such vacancy transfers may also be responsible for the increase of secondary ion yields with higher projectile charge, as was observed for impact of Ar^{q+} ($q = 1$–9) on a silicon surface.[27] Clear evidence that the fast projectile Auger electrons originate predominantly (i.e., to more than 90%) from below the surface was presented by scattering-angle-dependent data on K-Auger electron emission in collisions of N^{6+} and N^{7+} projectiles with clean metal surfaces.[18,19,25,34] For heavier MCI, filling of their inner-shell vacancies can also proceed via X-ray emission. Recently, considerably detailed information has been obtained from highly resolved

X-ray spectra produced in MCI–surface collisions.[22–24] In this way, complementary to the observation of fast Auger electron emission, the number of spectator electrons in higher principal quantum shells at the moment of a radiative inner-shell transition can be determined, which gives direct evidence for the existence of "hollow" projectiles even below the surface. Note, however, that the such produced X-ray photons can escape from much deeper layers in the solid than the fast Auger electrons, which must be taken into account for the comparison of results from both methods. The investigation of sequential Auger electron transitions during the subsequent recombination of two vacancies in the projectile K-shell has provided quantitative information on the involved transition time and consequently on the changing numbers of spectator electrons in outer shells.[34] Contributions by slow (< 50 eV) electrons originating either directly from b.s. processes (AN/AI) or produced as secondary electrons in collisions of the fast b.s. Auger electrons with bulk atoms and/or conduction electrons could so far not be separated from the a.s. slow electron contributions. However, a comparison of total slow electron yields for different projectile ion species with equal charge state (e.g., for impact of Ne^{9+} as compared to Ar^{9+} [33] or for Xe^{51+} as compared to Th^{51+} [35]) shows that in general more slow electrons are emitted for those projectile ions which carry fewer electrons. This seems to indicate the existence of b.s. slow-electron contributions to the total yield, since, according to our COB modelling calculations, the a.s. slow-electron emission, for a given projectile charge state, is insensitive to the actual projectile core.

(v) Projectile Backscattering

It is well known that slow ions after scattering from a clean metal surface leave the latter predominantly in the neutral state.[44] For impact of 20 keV Ne, Ar or Kr ions under 15° on a clean tungsten surface,[16,27] with primary charge states up to $q = 8$, only singly and doubly charged scattered projectiles could be observed, whereas for $q = 9$, triply charged scattered projectiles also showed up. This is a clear indication that inner-shell vacancies in the projectile have survived the backscattering and only thereafter became recom-

bined via Auger electron transitions on the outgoing projectile trajectory. Recently, it was demonstrated from the Doppler shift of K-shell Auger electron energies that for relatively fast, initially multicharged N^{6+}, O^{7+}, Ne^{9+} ions the Auger electron emission occurs mainly after projectile backscattering from the target surface.[20]

(vi) Comparison of Total Yields for Slow and Fast Electrons

As explained earlier, the major part of the fast Auger electrons produced due to MCI impact on metal surfaces will arise only after the projectile has entered the target bulk. The time available for a projectile above the surface is principally limited by its image charge acceleration. As an example, for N^{6+} impinging on clean tungsten, Eqs. (2) and (4) predict a time limit of about 80 femtoseconds. Moreover, the emission of a.s. K-shell electrons from the projectile is hampered because of the peculiar electronic population structure of the "hollow" projectile. On the other hand, after entering the target bulk, a nitrogen K-shell vacancy cannot survive longer than a few femtoseconds,[25,34] because the projectile L- and M-shells become quickly filled, which offers much more favorable conditions than given above the surface for the (most probable) KLL and KLM Auger transitions. Reference 34 gives further arguments for the observed preponderance of b.s. over a.s. fast Auger electron emission. It should be added that according to Eqs. (2) and (4) the image-charge acceleration-limited time interval, available for a projectile until its surface impact, slowly decreases with increasing initial charge state (in the high-q limit as $q^{-1/4}$). Whereas the small ratio between a.s. and b.s. fast Auger electron yields is well understood, almost no measurements have been made of complete electron energy spectra for MCI-induced PE from clean metal surfaces, except for normal incidence of N^{6+} and Ar^{9+} on clean polycrystalline tungsten.[40] At the respectively lowest impact energies (0.9 keV for N^{6+} and 1.35 keV for Ar^{9+}), the contribution of fast nitrogen K-shell electrons to the total electron yield was about 7% and that of the fast argon L-shell electrons about 1%, with the corresponding measured total electron yields being about 5.5[19,40] and 10 electrons per MCI,[14] respectively. Further evidence that the

fast Auger electron contribution to the total electron yields is indeed small can be deduced from corresponding absolute data given in the theses of de Zwart (Ar^{q+} on tungsten, $q \geq 9$; Ref. 16) and of Folkerts (H-like MCI of carbon, nitrogen and oxygen on tungsten; Ref. 19). In the latter work, at the respectively lowest impact energies of about 100 eV at 45° angle of incidence, thus giving "perpendicular" impact energies of about 50 eV, which however have to be increased by the respective image charge accelerations of about 12, 16 and 20 eV, respectively, the typical KLL Auger peak intensities rose up to about 4×10^{-3} electrons/(MCI.sr.eV). Some further analysis, taking into account the probable origin of b.s. Auger electrons inside the metal and their transport back into vacuum, shows that for each fast electron ejected per projectile K-shell vacancy inside the solid, typically only up to 0.3 fast electrons can actually escape and thus contribute to the total electron yield. This number has to be compared with the respective total electron yields to show that indeed the contributions from fast Auger electrons are relatively small. In Ref. 16 it has been shown that the number of fast Auger electrons originating from argon L-shell vacancy recombination is roughly proportional to the original number of vacancies. Considering the fact that when increasing the projectile charge state by one, the respective increments of the total slow electron yields are surely larger than one (see below, in particular Fig. 8), we conclude that the relative contribution of fast Auger electrons to the total yield will even gradually diminish toward higher charge states. However, despite the small fraction of fast Auger electrons, it should be stressed that a considerable part of the information now available in this field has been gleaned from their spectra.

If we assume that some of the b.s. fast Auger electrons produce secondary electrons inside the metal, consideration of the typical yields for such processes[45] under the given circumstances leads to about one slow b.s. electron for each scattered b.s. fast Auger electron. Consequently, the yields of b.s. slow secondary electrons and those of b.s. fast Auger electrons should be of comparable size and, therefore, the b.s. slow electron contributions will remain much smaller than the slow electron yields produced during phases (I)

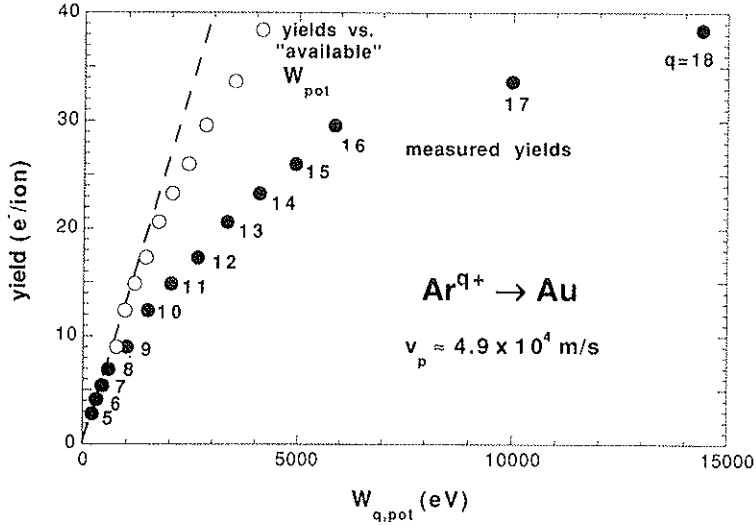

FIGURE 8 Measured total slow electron yields vs. total potential energy (full symbols) and "usable" potential energy (open symbols, cf. text), respectively, for 500 eV Ar^{q+} ($q \leq 18$) ions ($v_p \approx 4.9 \times 10^4$ m/s) impinging on clean gold (data from Refs. 33 and 35).

and (II), which in turn provide the by far dominant contributions to the total PE yields produced in slow MCI–metal surface collisions.

(vii) How Efficient Is the Total Potential Energy of Projectile Ions Spent for Electron Emission?

Finally we ask where the large potential energy brought in by a highly charged ion into a metal target will actually end up. As we have seen, for projectiles where during their neutralization in front of the surface inner-shell vacancies remain unfilled, a large part of their initial potential energy will be carried away by the resulting fast Auger electrons, which however does not greatly contribute to the total electron yield (see above). This is illustrated in Fig. 8, which presents measured total slow electron yields (which in the light of our above discussion are roughly equal to the respective total electron yields) for impact of 4.9×10^5 m/s Ar^{q+} (up to fully stripped ions) on clean polycrystalline gold[33,35] vs. the appropriate

total potential energies $W_{q,\mathrm{pot}}$ (sums of the respective single ionization potentials $W_{i-1,i}$ for $0 \leq i \leq q$). These ionization potentials, if calculated from Slater's rules,[46] agree within 5% with the results tabulated in Ref. 47. Ar ions in charge states $q \leq 8$ will keep completely filled K- and L-shells, whereas for $9 \leq q \leq 16$ a number of $(q-8)$ L-shell vacancies are present during the a.s. neutralization and, in addition, one/two K-shell vacancies for $Ar^{17+,18+}$. Given the limited time in front of the surface due to the projectile's image-charge acceleration (see above), all these $(q-8)$ inner-shell vacancies will survive practically until the surface impact and thus retain substantial excitation energy which is not available for a.s. emission of slow electrons in the course of the earlier outlined RN-AI-PO scenario. If we subtract the "withheld" excitation energy from the above-defined total potential energy $W_{q,\mathrm{pot}}$, the remaining part fits much better into a linear relation extrapolated from the respective total slow electron yields for $q \leq 8$ (cf. Fig. 8). For calculating these so-called "usable" potential energies, we have (optimistically) assumed that during the projectile neutralization until surface impact, electrons have already cascaded down into the respective M-shells. The still remaining discrepancy between the corrected potential energies and their linearly extrapolated values (dashed line in Fig. 8) indicates that with increasing q most of the a.s. captured electrons cannot actually make it down to the M-shell before surface impact. In addition, for $q = 17, 18$ a partial projectile deexcitation via X-ray emission could also be responsible for the discrepancies between the corrected values and the linear extrapolation.

SUMMARY

We have presented a rather complete scenario for the interaction of slow MCI with a metal surface, which is largely based on the now available experimental evidence. This scenario has been schematically summarized in Figs. 9a–9d. During phase I the MCI is accelerated towards the metal surface by its own image charge, and at a certain distance starts to extract electrons from the metal surface (Fig. 9a). These electrons are captured resonantly into highly ex-

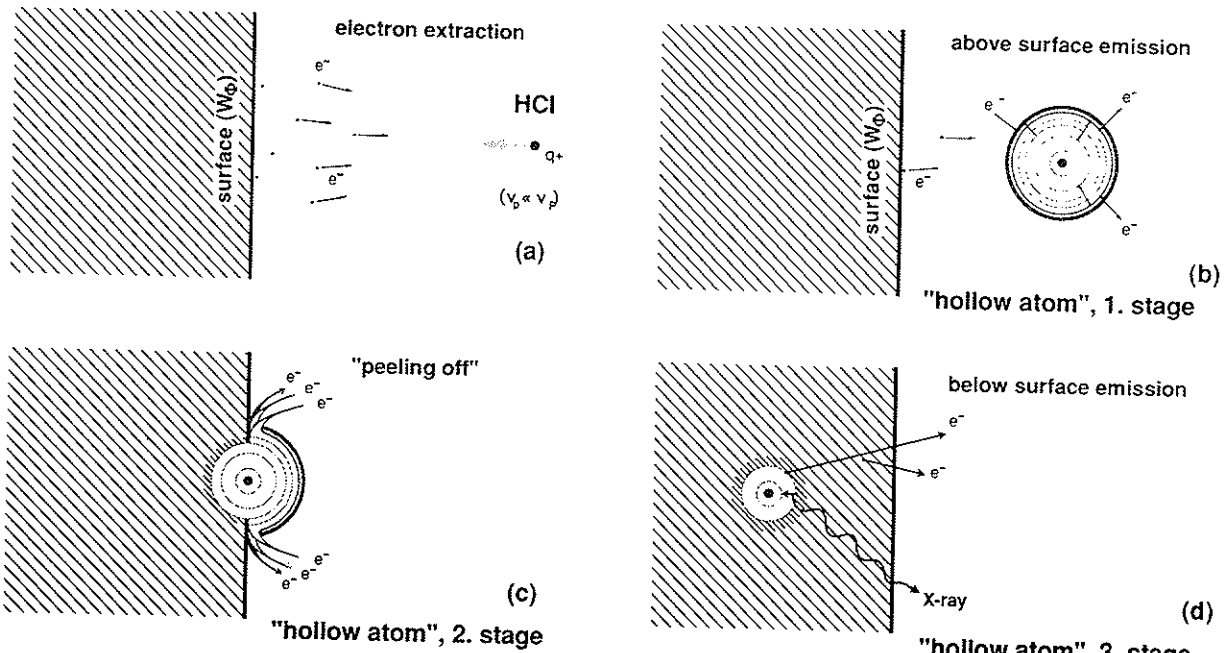

FIGURE 9 Processes initiated by the impact of a slow, highly charged ion on a clean metal surface (schematically). (a) Phase I, first electron extraction and resonant capture by the projectile. (b) Formation of a "hollow atom," which subsequently decays via autoionization and other above-surface electron emission mechanisms. (c) Screening of the projectile core by metal electrons causes "peeling-off" of weakly bound projectile electrons as soon as the projectile enters the solid. (d) Decay of inner-shell vacancies leads to emission of X-rays or fast Auger electrons, which subsequently can also produce slow (below surface) secondary electrons.

cited states of the projectile, eventually forming a neutral but "hollow atom," which subsequently decays via autoionization and other above-surface electron emission mechanisms (Fig. 9b). Because the image charge attraction limits the available interaction time, the autoionization cascade cannot be completed outside the solid. Screening of the projectile core by metal electrons upon surface impact results in the "peeling off" of the still weakly bound projectile electrons (Fig. 9c), which together with electrons resulting from the reneutralization of the projectile by Auger type processes will, at least partly, be emitted from the surface. Decay of still present inner-shell vacancies leads to emission of X-rays or fast Auger electrons, which subsequently can also produce slow (below surface) secondary electrons (Fig. 9d).

APPENDIX: LIST OF ABBREVIATIONS

AI	autoionization
AL	Auger loss to (empty states of) the conduction band
AN	Auger neutralization
a.s.	above surface
b.s.	below surface
COB	classical over-the-barrier (model)
ES	electron emission statistics
IS	image shift (of energy levels)
KE	kinetic electron emission
KLL	Auger transition combining a K-L transition with ionization of a second L electron
KLM	Auger transition combining a K-L transition with ionization of one M electron (not to be mixed up with the Dutch airline)
LEED	low energy electron diffraction
LMM	Auger transition combining an L-M transition with ionization of a second M electron
MCI	multicharged ion
PE	potential electron emission
PO	peeling-off
RI	resonant ionization

RN	resonant neutralization
S-DOS	surface density-of-states
SS	screening shift (of energy levels)

Acknowledgments

The authors thank H. Kurz for participation in the measurements, C. Lemell for performing the model calculations, Prof. J. Burgdörfer (University of Tennessee, USA) for valuable discussions on various aspects of the COB-model, Prof. R. Morgenstern (KVI Groningen, The Netherlands) for making Ref. 34 available prior to publication, Dr. H. Winter (University of Münster, Germany) for preliminary information about his Xe^{q+} data (Ref. 42), Dr. F. W. Meyer (Oak Ridge Natl. Lab., USA) for pointing out the possible production of b.s. slow electrons, and Dr. D. Schneider and co-workers (Lawrence Livermore Natl. Lab., USA) for a most fruitful cooperation. Various suggestions of the referees led to considerable improvement of the manuscript.

This work has been supported by Fonds zur Förderung der wissenschaftlichen Forschung (Proj. No. P8315TEC) and by Kommission zur Koordination der Kernfusionsforschung at the Austrian Academy of Sciences.

FRIEDRICH AUMAYR and HANNSPETER WINTER

Institut für Allgemeine Physik,
Technische Universität Wien,
Wiedner Hauptstrasse 8-10,
A-1040 Wien, Austria

References

1. H. D. Hagstrum, Phys. Rev. **96**, 325; 336 (1954).
2. J. W. Gadzuk, Surface Science **6**, 133; 159 (1967).
3. R. Brako and D. M. Newns, Surface Science **108**, 253 (1981).
4. P. Nordlander and J. C. Tully, Phys. Rev. Letters **61**, 990 (1988).
5. J. Los and J. J. C. Geerlings, Phys. Reports **190**, 133 (1990).
6. H. Winter, Comments At. Mol. Phys. **26**, 287 (1991).
7. H. D. Hagstrum and G. E. Becker, Phys. Rev. B **8**, 107 (1973).
8. P. Varga, W. Hofer and HP. Winter, J. Scanning Electron Microsc. **1**, 967 (1982).
9. P. A. Zeijlmans van Emmichoven, Thesis, University of Utrecht, The Netherlands (1989). P. A. Zeijlmans van Emmichoven and A. Niehaus, Comments At. Mol. Phys. **24**, 65 (1990).
10. H. Brenten, H. Müller and V. Kempter, Surf. Sci. **274**, 309 (1992).
11. K. Töglhofer, F. Aumayr and HP. Winter, Surf. Sci. **281**, 143 (1993).
12. H. D. Hagstrum, Phys. Rev. **104**, 672 (1956).
13. U. A. Arifov, L. M. Kishinevskii, E. S. Mukhamadiev and E. S. Parilis, Sov. Phys. Tech. Phys. **18**, 118 (1973).
14. M. Delaunay, S. Dousson, R. Geller, P. Varga, M. Fehringer and HP. Winter, *Book of Abstracts of 14th ICPEAC*, Palo Alto, USA, eds. M. J. Coggiola *et al.*, p. 477 (1985). M.

Delaunay, M. Fehringer, R. Geller, D. Hitz, P. Varga and HP. Winter, Phys. Rev. B **35**, 4232 (1987).
15. M. Delaunay, M. Fehringer, R. Geller, P. Varga and HP. Winter, Europhys. Lett. **4**, 377 (1987).
16. S. T. de Zwart, PhD thesis, Rijksuniversiteit Groningen (1987).
17. D. M. Zehner, S. H. Overbury, C. C. Havener, F. W. Meyer and W. Heiland, Surf. Sci. **178**, 359 (1986).
18. F. W. Meyer, S. H. Overbury, C. C. Havener, P. A. Zeijlmans van Emmichoven and D. M. Zehner, Phys. Rev. Lett. **67**, 723 (1991). F. W. Meyer, S. H. Overbury, C. C. Havener, P. A. Zeijlmans van Emmichoven, J. Burgdörfer and D. M. Zehner, Phys. Rev. A **44**, 7214 (1991). P. A. Zeijlmans van Emmichoven, C. C. Havener, I. G. Hughes, D. M. Zehner and F. W. Meyer, Phys. Rev. A **47**, 3998 (1993).
19. S. T. de Zwart, A. G. Drentje, A. L. Boers and R. Morgenstern, Surf. Sci. **217**, 298 (1989). L. Folkerts, PhD thesis, Rijksuniversiteit Groningen (1992). L. Folkerts and R. Morgenstern, Europhys. Lett. **13**, 377 (1990).
20. R. Köhrbrück, K. Sommer, J. P. Biersack, J. Bleck-Neuhaus, S. Schippers, P. Roncin, D. Lecler, F. Fremont and N. Stolterfoht, Phys. Rev. A **45**, 4653 (1992).
21. E. D. Donets, Physica Scripta **T3**, 11 (1983). E. D. Donets, Nucl. Instrum. Methods Phys. Res. Sect. B **9**, 522 (1985).
22. J. P. Briand, L. de Billy, P. Charles, S. Essabaa, P. Briand, R. Geller, J. P. Desclaux, S. Bliman and C. Ristori, Phys. Rev. Lett. **65**, 159 (1990).
23. H. J. Andrä *et al.*, in *Electronic and Atomic Collisions*, eds. W. R. MacGillivray, I. E. McCarty, and M. C. Standage (Adam Hilger, Bristol, 1992), p. 89.
24. M. W. Clark, D. Schneider, D. Dewitt, J. W. McDonald, R. Bruch, U. I. Safronova, I. Y. Tolstikhina and R. Schuch, Phys. Rev. A **47**, 3983 (1993). M. Schulz, C. L. Cocke, S. Hagmann, M. Stöckli and H. Schmidt-Böcking, Phys. Rev. A **44**, 1653 (1991).
25. S. T. de Zwart *et al.*, *loc. cit.* Ref. 19. F. W. Meyer, C. C. Havener, S. H. Overbury, K. J. Snowdon, D. M. Zehner, W. Heiland and H. Hemme, Nucl. Instrum. Meth. Phys. Res. B **23**, 234 (1987). S. Schippers, S. Hustedt, W. Heiland, R. Köhrbrück, J. Bleck-Neuhaus, J. Kemmler, D. Lecler and N. Stolterfoht, Phys. Rev. A **46**, 4003 (1992).
26. S. T. de Zwart, T. Fried, U. Jellen, A. L. Boers and A. G. Drentje, J. Phys. B: At. Mol. Opt. Phys. **18**, L623 (1985).
27. S. T. de Zwart, T. Fried, D. O. Boerma, R. Hoekstra, A. G. Drentje and A. L. Boers, Surf. Sci. **177**, L939 (1986); see also Ref. 16.
28. P. Varga, Appl. Phys. A **44**, 31 (1987). P. Varga, Comments At. Mol. Phys. **27**, 111 (1989).
29. H. J. Andrä, in *Physics of Highly-Ionized Atoms*, ed. R. Marrus (Plenum), NATO-ASI Series B: Physics Vol. 201, 377 (1989). H. J. Andrä, Nucl. Instrum. Meth. Phys. Res. B **43**, 306 (1989).
30. J. Burgdörfer, P. Lerner and F. W. Meyer, Phys. Rev. A **44**, 5674 (1991). J. Burgdörfer and F. W. Meyer, Phys. Rev. A **47**, R20 (1993). J. Burgdörfer, in *Progress in Atomic and Molecular Physics* (World Scientific), in press.
31. U. Wille, Phys. Rev. A **45**, 3004 (1992).
32. N. Vaeck and J. E. Hansen, J. Phys. B: At. Mol. Opt. Phys. **24**, L469 (1991).
33. H. Kurz, K. Töglhofer, HP. Winter and F. Aumayr, Phys. Rev. Lett. **69**, 1140 (1992). F. Aumayr, H. Kurz, K. Töglhofer and HP. Winter, Nucl. Instrum. Meth. Phys. Res. B **78**, 99 (1993).H. Kurz, F. Aumayr, C. Lemell, K. Töglhofer and HP. Winter, Phys. Rev. A **48** (1993), in press.
34. J. Das and R. Morgenstern, Phys. Rev. A **47**, R755 (1993). J. Das and R. Morgenstern, Comments At. Mol. Phys. (1993), in press.

35. F. Aumayr, H. Kurz, D. Schneider, M. A. Briere, J. W. McDonald, C. E. Cunningham and HP. Winter, Phys. Rev. Lett. (1993), in press.
36. G. Lakits, F. Aumayr and HP. Winter, Rev. Sci. Instrum. **60**, 3151 (1989). G. Lakits, F. Aumayr, M. Heim and HP. Winter, Phys. Rev. A **42**, 5780 (1990). F. Aumayr, G. Lakits and HP. Winter, Appl. Surf. Sci. **47**, 139 (1991).
37. P. Varga and HP. Winter, in *Particle Induced Electron Emission II*, ed. G. Höhler, Springer Tracts in Modern Physics **123**, 149 (1992).
38. H. Winter, Europhys. Lett. **18**, 207 (1992). H. Winter, Phys. Rev. A **46**, R13 (1992).
39. H. Winter, Comments At. Mol. Phys. **26**, 287 (1991). I. G. Hughes, C. C. Havener, S. H. Overbury, M. T. Robinson, D. M. Zehner, P. A. Zeijlmans van Emmichoven and F. W. Meyer, American Institute of Physics Conf. Proc. **274**, 610 (1993).
40. M. Fehringer, M. Delaunay, R. Geller, P. Varga and HP. Winter, Nucl. Instrum. Meth. Phys. Res. B **23**, 245 (1987). J. W. McDonald, D. Schneider, M. W. Clark and D. Dewitt, Phys. Rev. Lett. **68**, 2297 (1992).
41. A. Mazarro, P. M. Echenique and R. H. Ritchie, Phys. Rev. B **27**, 4117 (1983).
42. H. Winter, American Institute of Physics Conf. Proc. **274**, 583 (1993). H. Winter, C. Auth, R. Schuch and E. Beebe, submitted to Phys. Rev. Lett.
43. J. N. Bardsley and B. M. Penetrante, Comments At. Mol. Phys. **27**, 43 (1991).
44. H. Niehaus, W. Heiland and E. Taglauer, Surface Science Reports **17**, 213 (1993).
45. E. W. Thomas, in *Atomic and Plasma–Material Interaction Data for Fusion*, IAEA, Supplement to Nucl. Fusion **1**, 79 (1991).
46. J. C. Slater, Phys. Rev. **36**, 57 (1930).
47. R. L. Kelly and L. J. Palumbo, *Atomic and Ionic Emission Lines below 200 Ångstroms*, NRL Report 7599, Washington, D.C. (1973).